Airway microbiota signals anabolic and catabolic remodeling in the transplanted lung

Stéphane Mouraux, MD,[a]* Eric Bernasconi, PhD,[a]* Céline Pattaroni, MSc,[a] Angela Koutsokera, MD, PhD,[a] John-David Aubert, MD,[a] Johanna Claustre, MD,[b,c,d] Christophe Pison, MD, PhD,[b,c,d] Pierre-Joseph Royer, PhD,[e] Antoine Magnan, MD,[e] Romain Kessler, MD, PhD,[f] Christian Benden, MD, FCCP,[g] Paola M. Soccal, MD,[h] Benjamin J. Marsland, PhD,[a]‡ and Laurent P. Nicod, MD,[a]‡ on behalf of the SysCLAD Consortium§ *Lausanne, Zurich, and Geneva, Switzerland; and Grenoble, Saint Martin d'Hères, Nantes, and Strasbourg, France*

GRAPHICAL ABSTRACT

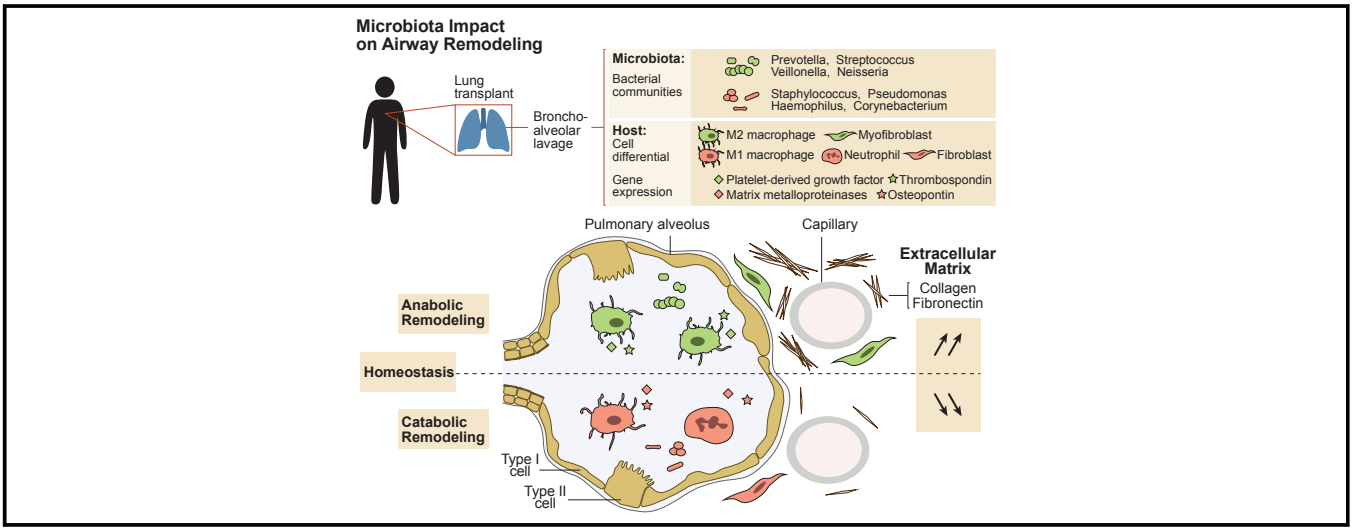

Background: Homeostatic turnover of the extracellular matrix conditions the structure and function of the healthy lung. In lung transplantation, long-term management remains limited by chronic lung allograft dysfunction, an umbrella term used for a heterogeneous entity ultimately associated with pathological airway and/or parenchyma remodeling.

Objective: This study assessed whether the local cross-talk between the pulmonary microbiota and host cells is a key

From [a]the Service de Pneumologie, Centre Hospitalier Universitaire Vaudois, Lausanne; [b]the Clinique Universitaire de Pneumologie, Pôle Thorax et Vaisseaux, Centre Hospitalier Universitaire Grenoble Alpes, Grenoble; [c]the Université Grenoble Alpes; [d]the Institut National de la Santé et de la Recherche Médicale 1055, Saint Martin d'Hères; [e]L'institut du Thorax, Service de Pneumologie, Centre Hospitalier Universitaire de Nantes, Institut National de la Santé et de la Recherche Médicale, Centre National de la Recherche Scientifique, Université de Nantes; [f]the Service de Pneumologie, Nouvel Hôpital Civil, Centre Hospitalier Universitaire, Strasbourg; [g]the Division of Pulmonology, University Hospital Zurich, Zurich; and [h]the Division of Pulmonary Medicine, Geneva University Hospitals, Geneva.

*These authors contributed equally to this work.

‡These authors contributed equally to this work.

§A full membership list of SysCLAD Consortium is published in this article's Online Repository at www.jacionline.org.

This work was supported by European Commission FP7 (grant no. 305457, SysCLAD Consortium), Swiss National Science Foundation (grant no. 156897, L.P.N.), Fondation de la Banque Cantonale Vaudoise (J.-D.A., E.B.), Fondation Juchum (S.M., A.K.), and Fondation Professeur Placide Nicod (C.Pa.). The Cohort of Lung Transplantation was financially supported by the Association Vaincre La Mucoviscidose, the Association Grégory Lemarchal, the Région Pays de La Loire, the Agence de Biomédecine, and the Institut Hospitalo-Universitaire CESTI. This work was realized in the context of the IHU-Cesti project thanks to French government financial support managed by the National Research Agency via the Investment into the Future program (ANR-10-IBHU-005). The IHU-Cesti project was also supported by Nantes Métropole and Région Pays de la Loire.

Disclosure of potential conflict of interest: S. Mouraux's institution received grant no. 305457, System prediction of Chronic Lung Allograft Dysfunction (SysCLAD) Consortium from European Commission FP7 and support for travel from American Thoracic Society for this work. E. Bernasconi's institution received grant no. 305457, SysCLAD Consortium from European Commission FP7; grant no. 156897 from Swiss National Science Foundation; and a grant from Fondation de la Banque Cantonale Vaudoise, Switzerland for this work. C. Pattaroni's, A. Koutsokera's, J.-D. Aubert's, J. Claustre's, C. Pison's, P.-J. Royer's, A. Magnan's, R. Kessler's, P. M. Soccal's, and B. Marsland's institutions received grant no. 305457, SysCLAD Consortium from European Commission FP7 for this work. C. Benden's institution received grant no. 305457, SysCLAD Consortium from European Commission FP7 and grant no. 156897 from Swiss National Science Foundation for this work; and he personally received consultancy fees from Astellas, Horizon Pharma, Gilead, and Vertex Pharmaceuticals; payment for lectures from Vertex Pharmaceuticals; and travel expenses from Astellas and CLS Behring. L. P. Nicod's institution received grant no. 305457, SysCLAD Consortium from European Commission FP7 and grant no. 156897 from Swiss National Science Foundation for this work. The authors declare that they have no relevant conflicts of interest.

Received for publication December 13, 2016; revised May 10, 2017; accepted for publication June 13, 2017.

Available online July 18, 2017.

Corresponding author: Eric Bernasconi, PhD, Service de Pneumologie, CLE D02-207, Chemin des Boveresses 155, 1066 Epalinges, Switzerland. E-mail: Eric.Bernasconi@chuv.ch.

The CrossMark symbol notifies online readers when updates have been made to the article such as errata or minor corrections

0091-6749

http://dx.doi.org/10.1016/j.jaci.2017.06.022

determinant in the control of lower airway remodeling posttransplantation.

Methods: Microbiota DNA and host total RNA were isolated from 189 bronchoalveolar lavages obtained from 116 patients post lung transplantation. Expression of a set of 11 genes encoding either matrix components or factors involved in matrix synthesis or degradation (anabolic and catabolic remodeling, respectively) was quantified by real-time quantitative PCR. Microbiota composition was characterized using 16S ribosomal RNA gene sequencing and culture.

Results: We identified 4 host gene expression profiles, among which catabolic remodeling, associated with high expression of metallopeptidase-7, -9, and -12, diverged from anabolic remodeling linked to maximal thrombospondin and platelet-derived growth factor D expression. While catabolic remodeling aligned with a microbiota dominated by proinflammatory bacteria (eg, *Staphylococcus*, *Pseudomonas,* and *Corynebacterium*), anabolic remodeling was linked to typical members of the healthy steady state (eg, *Prevotella*, *Streptococcus,* and *Veillonella*). Mechanistic assays provided direct evidence that these bacteria can impact host macrophage-fibroblast activation and matrix deposition.

Conclusions: Host-microbes interplay potentially determines remodeling activities in the transplanted lung, highlighting new therapeutic opportunities to ultimately improve long-term lung transplant outcome. (J Allergy Clin Immunol 2018;141:718-29.)

Key words: *Airway remodeling, fibroblasts, macrophages, matrix, microbiota*

Despite a marked improvement over the last 2 decades, lung transplantation remains associated with a lower survival rate (54% at 5 years posttransplantation in 2013),[1] compared with the rates for heart, kidney, liver, and pancreas transplantations. In fact, long-term management of the lung allograft faces a major, as yet incompletely characterized condition: chronic lung allograft dysfunction (CLAD), an umbrella term used to describe different phenotypes of chronic lung allograft rejection, for which a general consensus on the precise clinical definition is still lacking. The heterogeneity of CLAD phenotypes reflects the complexity of the underlying mechanisms, whereby inflammation combined with aberrant airway and/or parenchyma remodeling progressively impairs lung function, ultimately leading to retransplantation or death.[2] Consequently, there is an urgent need for increasing our understanding of CLAD pathophysiology and identifying biomarkers that are specific for the different CLAD phenotypes.

A rich and balanced airway microbiota has been linked with the maintenance of local tissue homeostasis. Perturbation in the composition of this microbial community, known as dysbiosis, has been reported in a variety of respiratory conditions, including lung transplantation.[3-6] We recently showed that there is a predominance of proinflammatory (eg, *Staphylococcus* and *Pseudomonas*) or low stimulatory (eg, *Prevotella* and *Streptococcus*) bacteria aligned with inflammatory or tissue remodeling gene expression profiles, respectively, in bronchoalveolar lavage (BAL) cells following transplantation, which suggests that the pulmonary microbiota may impact long-term graft survival.[7]

In the present study, we sought to dissect host-microbe interactions in the context of the complex remodeling processes taking place following lung transplantation. We show that the transplanted lung presents distinct remodeling profiles, characterized by the expression of genes differentially involved in matrix synthesis or degradation. In addition, we provide evidence that the constituents of microbial communities dominated by these bacterial taxa fine-tune gene expression profiles in macrophages and fibroblasts—2 key cell types in the regulation of remodeling processes.

Abbreviations used

BAL:	Bronchoalveolar lavage
CFU:	Colony-forming unit
CHI3L1:	Chitinase 3-like 1
CLAD:	Chronic lung allograft dysfunction
COPD:	Chronic obstructive pulmonary disease
GO:	Gene Ontology
IGF:	Insulin-like growth factor
IQR:	Interquartile range
KEGG:	Kyoto Encyclopedia of Genes and Genomes
KO:	KEGG ortholog
MMP:	Matrix metallopeptidase
PDGFD:	Platelet-derived growth factor D
rRNA:	Ribosomal RNA
SPP1:	Secreted phosphoprotein 1
SysCLAD:	System prediction of Chronic Lung Allograft Dysfunction
THBS1:	Thrombospondin 1
THP-DM:	THP1-derived macrophages

METHODS

Patient sample collection and ethics statement

BAL samples were collected during surveillance bronchoscopies carried out during the first 14 months posttransplantation, from October 2012 to July 2014 in 6 Swiss and French transplantation centers, within the framework of the European project System prediction of Chronic Lung Allograft Dysfunction (SysCLAD).[8] The national and local ethics committees approved the study, and all subjects, whose details are provided in Table I,[9] gave written informed consent.

Detail on BAL fluid collection and processing is provided in the Methods in this article's Online Repository (available at www.jacionline.org). BAL fluid was submitted to cell differential determination, culture-dependent bacterial and fungal detection, and PCR-based detection of viral infection, according to routine clinical procedures. Negative control samples obtained on washing a ready-to-use endoscope with sterile saline were prepared following the same procedure.

RNA-seq and data analysis

Total BAL cellular RNA converted into cDNA libraries using the Illumina TruSeq RNA Sample Preparation Kit (Illumina, San Diego, Calif) was submitted to high throughput sequencing using the Illumina HiSeq 2500 System. Gene expression quantification was based on reads per kilobase of exon model per million mapped reads.

Extraction of remodeling genes from Gene Ontology database

A panel of 627 remodeling-related genes were extracted from Gene Ontology (GO) database (release May 2016) using the browser AmiGo[10] (version 2.3), based on GO Terms listed in Fig 1, *B*.

TABLE I. Patient characteristics

Patients/samples	Total, no.	116/189
	Male	58 (50.0)
	Age at transplant (y)	52 (35, 61)
	Sampling time point (days posttransplantation)	339 (92, 376)
Type of transplant	Bilateral lung	101 (87.0)
	Single lung	15 (12.9)
Pretransplantation diagnosis	Chronic obstructive pulmonary disease	38 (32.8)
	Cystic fibrosis	31 (26.7)
	Interstitial lung disease	24 (20.7)
	Graft failure (retransplantation)	5 (4.3)
	Other	18 (15.5)
Transbronchial biopsies*†		167 (88.4)
	A0	128 (76.6)
	A1	21 (12.6)
	A2	5 (3.0)
	B0	105 (62.9)
	B1	19 (11.4)
	B2	1 (0.6)
Immunosuppression*	Tacrolimus	176 (93.1)
	Cyclosporin	13 (6.9)
Antibiotics*	TMP/SMX	143 (75.7)
	Azithromycin	25 (13.2)
	Other (inhaled, oral, or intravenous routes)	54 (28.6)
BAL positive bacterial culture (excludes oropharyngeal flora)*	*Staphylococcus aureus* (n = 10), *Pseudomonas aeruginosa* (n = 10), *S epidermidis* (n = 5), *Corynebacterium* sp (n = 4), *Enterococcus* sp (n = 3), *Streptococcus* sp (n = 1), *Klebsiella pneumoniae* (n = 1), *Haemophilus influenzae* (n = 1), *Escherichia coli* (n = 1), *Enterobacter* sp (n = 1)	32 (16.9)
BAL positive fungal culture*	*Aspergillus* sp (n = 4), *Penicillium* sp (n = 3), *Candida* sp (n = 4)	13 (6.9)
BAL positive viral PCR*‡	CMV (n = 11), EBV (n = 2), metapneumovirus (n = 1), parainfluenza (n = 1)	14 (13.2)

Data presented as n (% of group) or median (IQR) unless otherwise indicated.
CMV, Cytomegalovirus; *TMP/SMX*, trimethoprim/sulfamethoxazole.
*At sampling.
†Grading of pulmonary allograft rejection according to guidelines of the International Society for Heart and Lung Transplantation.[9]
‡Conducted in a subset (n = 106) of samples. Virological investigations ranged from CMV only to more extensive testing, as per case requirement.

Real-time quantitative PCR for characterizing gene expression profiles

BAL cellular RNA was extracted, cDNA synthesized, and amplification performed using custom oligonucleotide primers and probes (Microsynth, Balgach, Switzerland; see details in the Methods and Table E1 in this article's Online Repository at www.jacionline.org).

Bacterial 16S ribosomal RNA gene amplification, sequencing, and metagenome prediction

The 16S content of BAL fluid DNA was characterized either by quantitative PCR using previously reported primers specific to pan bacteria or by major phyla (Bacteroidetes, Firmicutes, Proteobacteria, Actinobacteria, and Fusobacteria), or Illumina MiSeq sequencing using primers targeting the V1-V2 region, as previously described.[11] Sequences were processed and the resulting table of operational taxonomic units was used for metagenome prediction, using Phylogenetic Investigation of Communities by Reconstruction of Unobserved States (PICRUSt) software[12] (see detail in the Methods in this article's Online Repository).

Bacterial cultures

Culture conditions for *Staphylococcus aureus* (ATCC 25904; ATCC, Manassas, Va), *Pseudomonas aeruginosa* (ATCC BAA-47), *Streptococcus pneumoniae* (NCTC 7466; Public Health England, Salisbury, UK), and *Prevotella melaninogenica* (ATCC 25845) are provided in the Methods in this article's Online Repository. For stimulation experiments, suspensions were diluted to reach a concentration of 4×10^{-3} (*P aeruginosa* and *S pneumoniae*) or 2×10^{-3} (*S aureus* and *P melaninogenica*) optical density at 600 nm corresponding to 10^6 colony-forming units (CFUs) per milliliter.

In vitro macrophage-fibroblast coculture model of matrix deposition

Conditions for maintenance of human THP-1 monocytic cell line (ATCC TIB-202) and MRC-5 fibroblasts (ATCC CCL-171), and macrophage colony-stimulating factor 1-driven generation of THP-1-derived macrophages (THP-DM) are provided in the Methods in this article's Online Repository. Stimulation using the bacterial suspensions described above, at a density of 5 CFUs per eukaryotic cell at day 0, was performed for 30 hours (gene expression analysis) or 6 days (quantification of matrix deposition) in minimum essential medium (Thermo Fisher Scientific, Rochester, NY), supplemented with 70- and 400-kDa Ficoll (37.5 and 25 mg/mL, respectively; GE Healthcare, Little Chalfont, UK) and transforming growth factor-β1 ([TGF-β1], 5 ng/mL; eBioscience, San Diego, Calif) for optimal matrix deposition, along with a mixture of prednisolone (500 nmol/L; Sigma, St Louis, Mo)/FK506 (tacrolimus, 25 nmol/L; Enzo Life Sciences, Lausen, Switzerland)/mycophenolic acid (10 μmol/L; Tocris Bioscience, Ellisville, Mo). Penicillin and streptomycin (1000 U/mL and 100 μg/mL, respectively; Thermo Fisher Scientific) were used to prevent bacterial growth, and cell viability was assessed using a dedicated colorimetric assay (Cell Counting Kit-8, Dojindo Molecular Technologies, Rockville, Md). Immunostaining for collagen type 1 and fibronectin and automated image acquisition are detailed in the Methods in this article's Online Repository.

Principal component and statistical analysis

To analyze the distribution of BAL cell gene expression profiles, the target gene/reference gene copy number ratio was log-transformed and principal component analysis was performed using prcomp (scaled) routine in R (R Foundation, Vienna, Austria).[13] Multiple-group comparisons were performed using Kruskal-Wallis test with Dunn *post hoc* analysis and

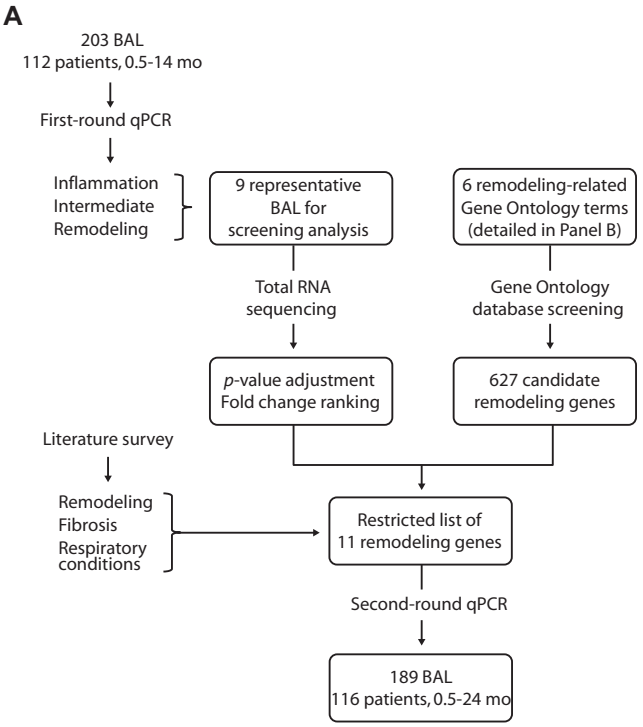

B

Category	Gene Ontology term	Associated gene number
Growth factors	Transforming growth factor	175
	Platelet-derived growth factor	33
Remodelling	Extracellular matrix	415
	Tissue remodeling	8
Matrix components	Collagen	133
	Fibronectin	20

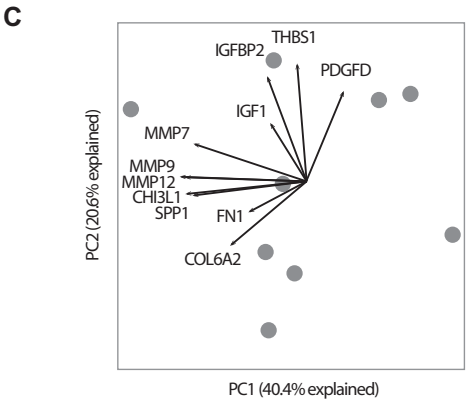

FIG 1. Identification of a set of remodeling genes. **A,** Schematic outline of experimental approach. **B,** GO criteria used in candidate gene selection process. **C,** Principal component (*PC*) analysis, and associated eigenvectors, based on quantitative PCR determination of expression of the restricted list of 11 remodeling genes (see Table II for details) in the initial subset of 9 BAL samples (*dots*).

posttransplantation differences in the relative abundance of the remodeling gene expression profiles were compared using chi-square test (R package PMCMR). In metagenomic prediction analysis, statistical significance was evaluated using DESeq2 package in R (P value < .05; $\log_2$ fold-change >2). Graphs were generated using Prism 6.0 software (GraphPad, La Jolla, Calif).

RESULTS

Experimental toolkit for determining remodeling gene expression profiles in BAL cells

In a previous study, we showed that a majority of BAL samples obtained from lung transplant recipients up to 14 months posttransplantation can be distinguished on the basis of the expression levels of a set of genes involved in inflammation and remodeling.[7] However, a substantial group representing 43% of total samples showed an intermediate profile and remained poorly characterized. Moreover, we noted an overlap across the whole sample set in the expression of the selected remodeling markers—platelet-derived growth factor D (PDGFD) and the tissue inhibitor of metallopeptidase 1/matrix metallopeptidase 12 (MMP12) ratio. These data highlighted the need to develop an analytical toolkit able to further dissect the complexity of remodeling gene expression profiles posttransplantation.

To this end, we employed 2 complementary approaches (experimental scheme detailed in Fig 1, *A*). A subset of 9 BAL samples, that represented an inflammatory, remodeling, or intermediate gene expression profile in our first-round real-time PCR, was analyzed by RNA sequencing. Data were filtered on the basis of adjusted P value (.05 threshold) and ranked by fold-change. In parallel, we selected 6 GO terms linked to remodeling (see Fig 1, *B* for details) and interrogated the GO database using the application AmiGO version 2.3,[10] generating a list of 627 candidate genes. Table II presents the restricted list of 11 remodeling genes obtained after combining the 2 approaches, and further assessing potential candidates on the basis of a literature survey on the remodeling-fibrosis axis, in the context of various respiratory conditions. Real-time PCR validation analysis indicated that expression of the selected genes in our initial set of 9 BAL samples was associated with a widespread distribution of corresponding eigenvectors, as obtained by principal component analysis, consistent with implications in diverse remodeling-related activities (Fig 1, *C*). Indeed, the corresponding encoded proteins have been linked to multiple aspects of remodeling, including matrix composition, accumulation and degradation.[14-21]

Four host remodeling gene expression profiles prevail in the transplanted lung

To gain further insight into remodeling gene expression profiles posttransplantation, we analyzed by real-time PCR 189 BAL samples obtained from 116 patients between 0.5 and 24 months posttransplantation (see Table I for details)[9] using our new analytical toolkit. Principal component analysis (Fig 2, *A*) and hierarchical clustering (Fig 2, *B*) allowed us to identify 4 profiles that we defined as low, intermediate, anabolic, and catabolic remodeling, representing 21%, 47%, 20%, and 12% of total samples, respectively. Per-gene analysis confirmed that the low and intermediate groups were indeed associated with low and intermediate expression levels, respectively, of virtually all genes

TABLE II. Remodeling gene set used for the characterization of BAL cell profiling*

Gene name, alias†	Gene symbol†	Molecular functions
Chitinase 3-like 1	CHI3L1	Regulator of cell-matrix interactions
Collagen type VI α-2 chain	COL6A2	Matrix constituent
Fibronectin 1	FN1	Matrix constituent
Insulin-like growth factor 1	IGF1	Fibroblast proliferation and activation
Insulin-like growth factor binding protein 2	IGFBP2	Fibroblast proliferation and activation
Matrix metallopeptidase 7	MMP7	Mediator of matrix turnover; basement membrane proteolysis
Matrix metallopeptidase 9	MMP9	Mediator of matrix turnover; collagen and fibronectin proteolysis
Matrix metallopeptidase 12	MMP12	Mediator of matrix turnover; elastin proteolysis
Platelet-derived growth factor D	PDGFD	Fibroblast proliferation and survival
Secreted phosphoprotein 1, osteopontin	SPP1	Regulator of cell-matrix interactions
Thrombospondin 1	THBS1	Regulator of cell-matrix interactions; major activator of TGF-β1

*Primer and probe sequences are available in Table E1 in this article's Online Repository.
†According to Human Gene Organization (HUGO) Gene Nomenclature Committee at the European Bioinformatics Institute.

tested (Fig 2, *C*). Anabolic remodeling was characterized by maximal expression of thrombospondin 1 (THBS1) and PDGFD, 2 factors previously linked to TGF-β-mediated repair in different experimental and clinical settings (Fig 2, *C*).[20,22] In contrast, expression of several metallopeptidases (MMP7, MMP9, and MMP12), typically associated with inflammation and matrix degradation, distinguished the catabolic remodeling group. This latter profile was also linked to a high expression of additional remodeling markers, including the matrix constituents collagen type VI α-2 and fibronectin 1, the growth-promoting insulin-like growth factor 1 (IGF1), and the matricellular proteins osteopontin (secreted phosphoprotein 1 [SPP1]), chitinase 3-like 1 (CHI3L1), and IGF binding protein 2, all involved in the regulation of matrix turnover (Fig 2, *C*). Spearman correlation analysis confirmed these associations, with a coefficient (ρ) ranging from -0.27 (PDGFD vs SPP1) to 0.78 (MMP9 vs CHI3L1) indicating negative and positive correlation, respectively (see Fig E1 in this article's Online Repository at www.jacionline.org).

We next observed that the different remodeling gene expression profiles identified were linked to distinct kinetics following transplantation ($P < .05$ by chi-square test) (Fig 2, *D*). Specifically, low remodeling was almost limited to the first 12 months posttransplantation, while the intermediate profile predominated in each of the 4 time windows considered (Fig 2, *D*). We further observed that catabolic remodeling peaked between 3 and 6 months, clearly preceding the maximal relative frequency of anabolic remodeling, from 12 months onward (Fig 2, *D*). This latter divergence in the kinetics of catabolic versus anabolic remodeling was confirmed when we considered 87 combinations of paired samples obtained from 34 patients, who were lavaged multiple times (median: 3, range: 2-6) (Fig 2, *E* and Table E2 in this article's Online Repository). A schematic representation of these longitudinal transitions between 2 different remodeling profiles further highlighted the marked difference between the catabolic and anabolic profiles, testified by a single direct transition (Fig 2, *F*). In contrast, the intermediate remodeling profile was often connected to either the low, anabolic, or catabolic remodeling profile, which is consistent with a central position (Fig 2, *F*). Furthermore, we observed a substantial degree of stability in remodeling gene expression over time. Indeed, 34 paired samples (39%) were linked to a stable profile, while 52 others (61%) showed a profile transition. Moreover, when further focusing on 14 patients who provided from 4 to 6 BAL samples (median: 4.5, interquartile range [IQR]: 4, 5) over a range of 5.5 to 21 months (see details in Table E2 in this article's Online Repository at www.jacionline.org), we found a median number of 2 profiles (IQR: 2.0, 2.3). Here, the relative frequency of paired samples with a stable profile decreased from the intermediate, anabolic, catabolic, to low remodeling background (50%, 23%, 15%, and 12%, respectively). Overall, these observations support the existence in the transplanted lung of distinct remodeling activities, differentially interconnected, and regulated in a time-dependent manner.

Relation between airway microbiota composition and host remodeling gene profiling

We previously reported that the airway microbiota composition varies in concert with BAL cell gene profiling posttransplantation.[7] In particular, we showed that dysbiosis, defined by a strong predominance of a single phylum exceeding 70% of relative abundance, was associated with a high expression of 2 contrasting sets of genes, linked to either inflammation or remodeling, depending on the predominant phylum, while more balanced bacterial communities aligned with a neutral gene expression profile. We therefore investigated whether the airway microbiota composition aligned with the 4 host remodeling gene expression profiles identified in the present study, with a special interest in the contrasting catabolic and anabolic profiles. For this purpose, we relied on a combination of molecular analysis and culture, which proved complementary in distinguishing the composition of the airway microbiota associated with a catabolic remodeling gene expression profile, versus that linked to a low, intermediate, or anabolic profile. Specifically, PCR amplification of the 16S ribosomal RNA (rRNA) gene using phylum-specific primers indicated that dysbiosis observed in 37% of total BAL samples was increased when driven by Firmicutes or Actinobacteria, and decreased when Bacteroidetes predominated, on a catabolic remodeling background (Fig 3, *A*). Moreover, sequence analysis at genus level underscored the association of catabolic remodeling with *Staphylococcus*, *Corynebacterium*, *Stenotrophomonas,* and *Haemophilus* (Fig 3, *B*). In contrast, a microbial community comprising *Prevotella*, *Streptococcus*, *Veillonella,* and *Neisseria* was poorly represented in this catabolic remodeling context, while strongly predominating in association with low,

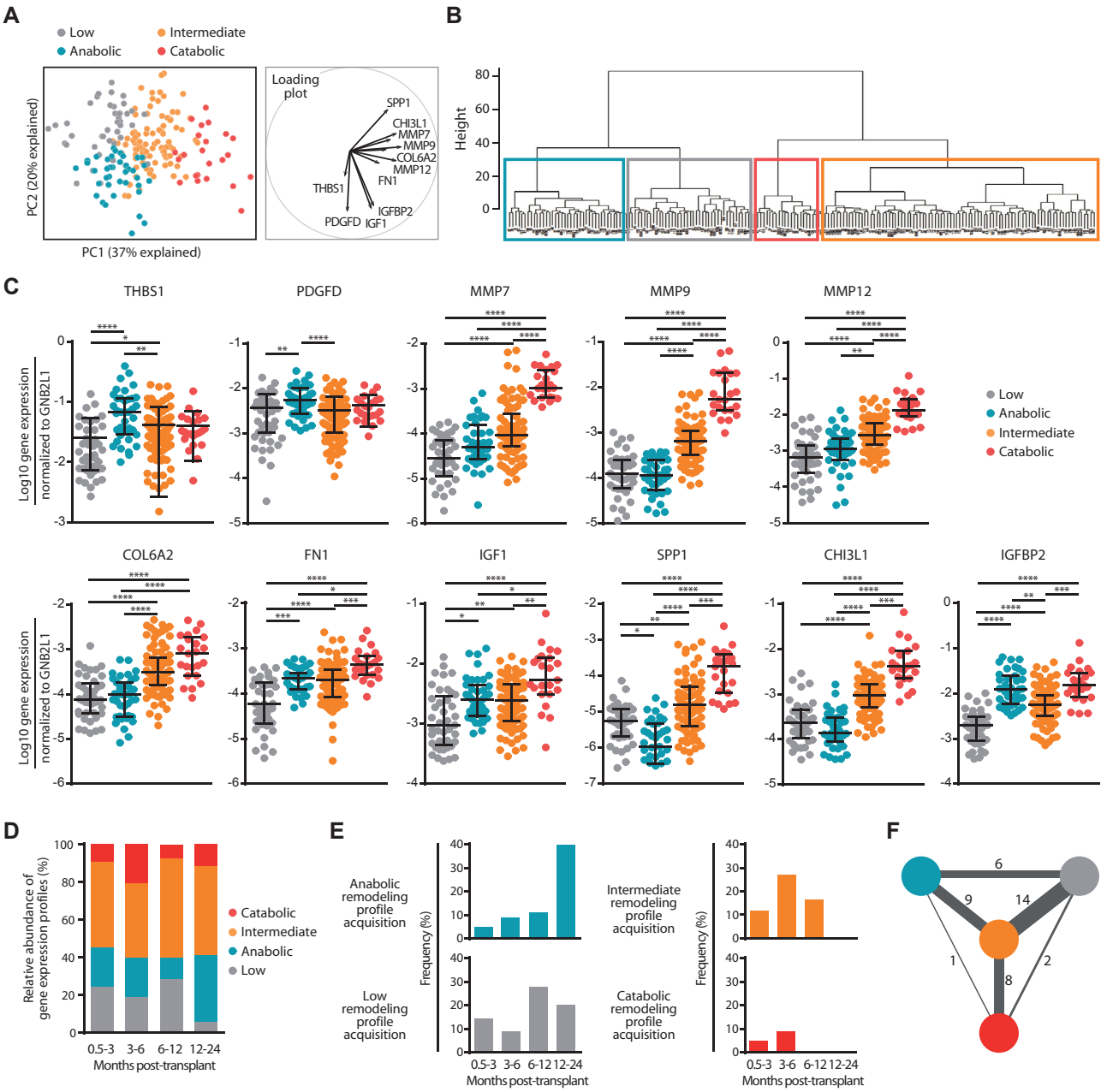

FIG 2. Identification of 4 remodeling gene expression profiles in posttransplantation BAL samples. PC analysis **(A)** and hierarchical clustering **(B)** based on qPCR determination of gene expression **(C)**. Medians and IQRs are indicated. *$P < .05$, **$P < .01$, ***$P < .001$, and ****$P < .0001$. Transversal **(D)** and intraindividual **(E)** posttransplantation variations in remodeling gene expression profile. **E,** Data show the frequency of sample pairs that displayed acquisition of a new remodeling profile. **F,** Schematic diagram of intraindividual remodeling profile transitions with indicated occurrences.

intermediate, or anabolic remodeling (Fig 3, *B*). These specificities in the airway microbiota composition linked to host catabolic remodeling gene expression profiling were also accompanied by a reduced diversity compared with the 3 other remodeling profiles (Fig 3, *C*).

Assessment of positive cultures confirmed *Staphylococcus* spp and *Corynebacterium* spp, and additionally included *Pseudomonas* spp, as part of the bacteria primarily linked to a catabolic remodeling profile (Fig 3, *D*). In contrast, BAL samples tested positive for oropharyngeal flora, which typically includes bacteria of the genera *Prevotella*, *Streptococcus*, *Veillonella,* and *Neisseria*,[3] predominated in association with an anabolic remodeling gene expression profile (Fig 3, *D*).

To explore further the links between the airway microbiota composition and host gene expression, and given the early onset of the catabolic remodeling profile, versus the late onset of the anabolic remodeling profile, we next determined the relative abundance of the different microbiota states within 4 time windows posttransplantation (Fig 3, *E*). Here, we found that microbiota dysbiosis was more likely to occur during the first 6 months posttransplantation when driven by Firmicutes, while becoming more frequent over time when driven by Bacteroidetes,

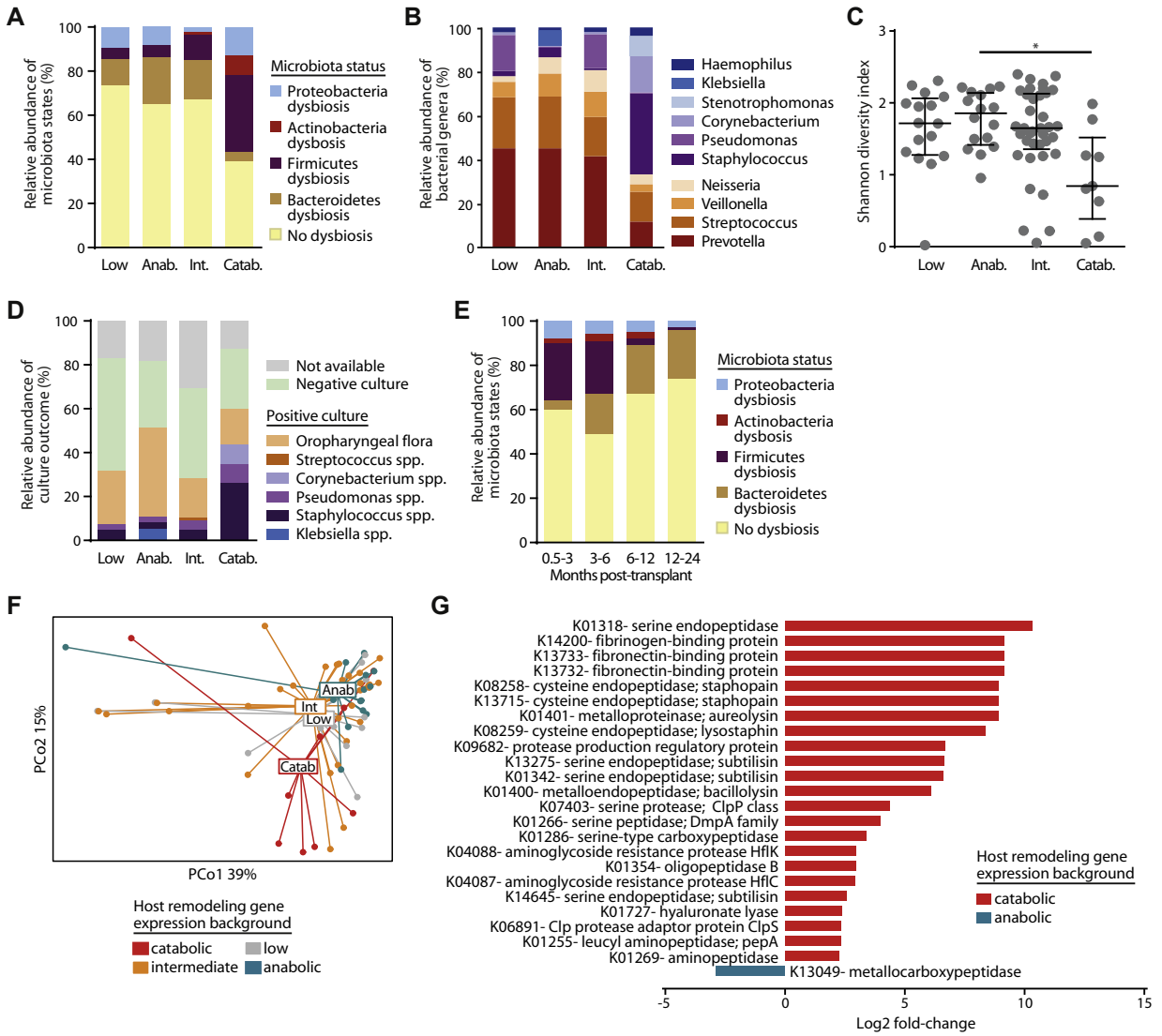

FIG 3. Associations between the pulmonary microbiota and host remodeling gene expression. Microbiota status **(A)**, the 10 most abundant microbial genera **(B)**, Shannon diversity index with medians and IQRs, **P* < .05 **(C)** and culture outcome **(D)** as per remodeling profile. **E,** Kinetics of microbiota status posttransplantation. **F,** Bray-Curtis principal coordinate (*PCo*) analysis of inferred metagenomic content. **G,** Differential abundance analysis focused on KOs related to bacteria-matrix interaction or proteolysis, on a catabolic versus anabolic remodeling gene expression background.

thus aligning with the kinetics of catabolic and anabolic remodeling, respectively. Furthermore, we applied PICRUSt analysis to gain insight on the predictive metagenome functions of the bacterial communities linked to the 4 remodeling profiles.[13] PICRUSt links operational taxonomic units, as identified by 16S rRNA gene sequencing, to Kyoto Encyclopedia of Genes and Genomes (KEGG) genes, their corresponding KEGG orthologs (KOs) and, ultimately, functions. Global analysis of the predicted metagenome indicated a segregation of the microbial communities found on a catabolic remodeling background, which especially differed from the communities associated with an anabolic remodeling profile (Fig 3, *F*). To investigate potential differences with respect to host remodeling more specifically, we next considered a subset of 159 KOs related to bacteria-matrix interaction and/or protein degradation. We found that 24 genes were significantly differentially represented (threshold set to $\log_2$ fold-change >2) within the communities associated with a catabolic, compared with an anabolic, remodeling profile (Fig 3, *G*). Of note, 23 of those genetic markers, which included, however not exclusively, virulence factors linked to infections of various etiology, including *S aureus* and *P aeruginosa*, were enriched (median $\log_2$ fold-change: 6.1, IQR: 2.3, 10.3; adjusted *P* value ≤ .01) in the communities associated with a catabolic remodeling profile (Fig 3, *G*).

Host-microbe associations and the underlying clinical situation

The relatively limited follow-up time in our study did not allow us to look for associations between the observed features in host remodeling gene expression or microbiota composition and the onset of chronic rejection. Moreover, we found no link with the

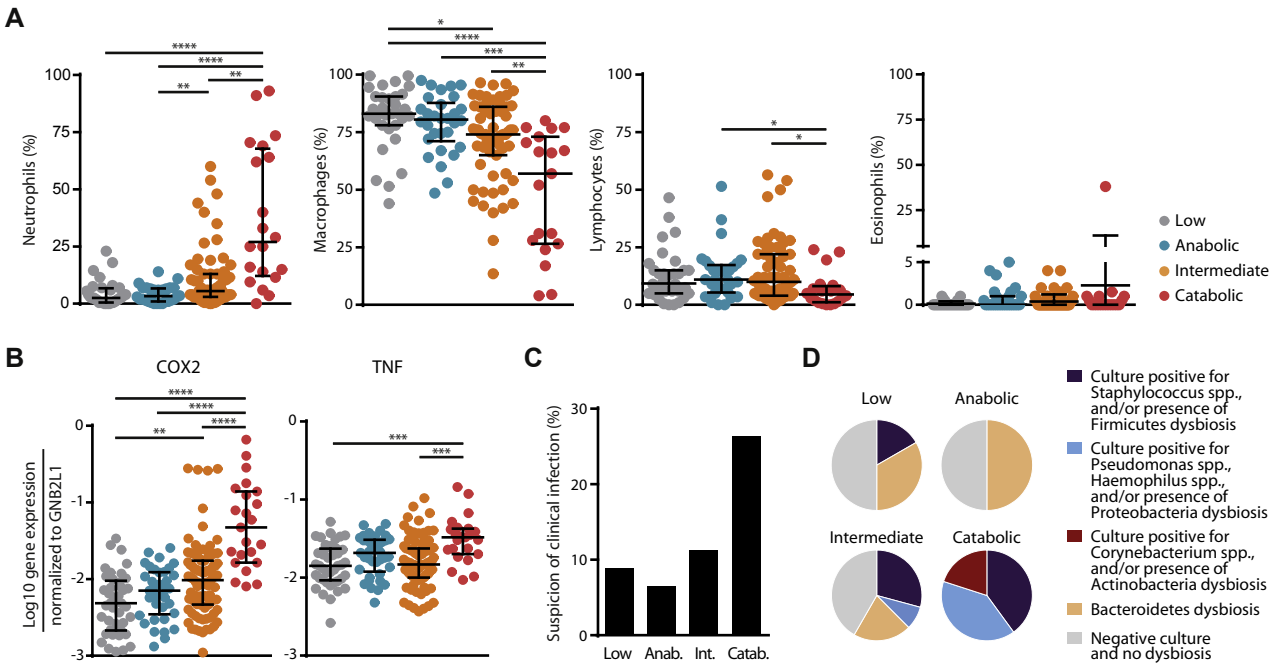

FIG 4. Associations among host remodeling, inflammation, and infection. Relationship among host remodeling and BAL cell differential **(A)**, expression of inflammatory genes COX2 and TNF-α **(B)**, prevalence of suspected clinical infection **(C)**, and bacteria isolated by culture and/or driving dysbiosis **(D)**. In panels **A** and **B**, medians and IQRs are indicated. **P* < .05, ***P* < .01, ****P* < .001, and *****P* < .0001.

diagnosis of acute cellular rejection (A grade), as established on histologic analysis of transbronchial biopsies (see Table E3 in the Online Repository at www.jacionline.org). In addition, when considering samples with a histologic diagnosis of airway inflammation (lymphocytic bronchiolitis, B grade), we found only a slight increase between the percentage of samples with a catabolic remodeling signature versus those of samples with a low, intermediate, or anabolic profile (21.4% vs 11.4%, 10.9%, and 15.4%, respectively) (see Table E3 in the Online Repository). However, confirming our previous findings,[7] Firmicutes-, Proteobacteria-, and Actinobacteria-driven dysbiosis, rather than the absence of dysbiosis or Bacteroidetes-driven dysbiosis, was found to be linked to histologically determined airway inflammation (27.8%, 15.9%, and 4.8%, respectively) (see Table E3 in the Online Repository).

To assess potential links among host remodeling, microbiota states, and inflammation directly in the BAL, we next looked at the cell differential and found a marked enrichment in neutrophils, a hallmark of acute inflammation, accompanied by a corresponding relative decrease in macrophage and lymphocyte counts, on a catabolic remodeling background (Fig 4, *A*). Consistently, we also observed a stronger expression of the inflammation marker genes COX2 and TNF-α (Fig 4, *B*) in this setting. These observations suggested that the microbial communities linked to catabolic remodeling exhibit increased inflammatory properties in comparison to the principal members of the community dominated by *Prevotella*,[7,23] as previously reported.

Given that the bacterial genera associated with catabolic remodeling comprise common respiratory pathogens, we next aimed to evaluate the links between host remodeling-microbe associations and the diagnosis of infection. For this purpose, we focused our attention on a subset of 29 BAL samples obtained from patients who presented with clinical evidence of infection and had a positive result in BAL culture by routine microbiological examination and/or microbiota dysbiosis detected by 16S rRNA gene amplification. BAL samples with catabolic and anabolic remodeling gene expression profiles aligned with maximal and minimal rates of clinical infection, respectively (Fig 4, *C*). Moreover, when considering all of those samples associated with a clinical suspicion of infection, we found a striking difference in the bacteria identified by culture and/or type of detected dysbiosis, depending on the remodeling context (Fig 4, *D*). Hence, combined with the information we obtained on the kinetics of gene expression profiles (Fig 2, *D* and *E*) and microbiota states (Fig 3, *E* and *F*), this dataset indicated that the early acquisition of a catabolic remodeling profile and dysbiosis driven by highly stimulatory bacteria, is linked to inflammation and a more frequent association with clinical infection. In contrast, the clinical implications of the coincident anabolic remodeling profile and dysbiosis driven by low stimulatory bacteria, which are likely to be expressed later following lung transplantation, remain to be defined.

The constituents of airway microbial communities set the balance between anabolic and catabolic remodeling

The identification of anabolic and catabolic gene expression profiles linked to different airway microbiota compositions raised the possibility that the extracellular matrix turnover in the transplanted lung is differentially influenced by the constituents of local bacterial communities. To address this, we used an *in vitro* model system that exploits the microbial sensing and proremodeling capacities of THP-DM and MRC-5 fibroblasts to compare the direct effects of bacterial mixes on remodeling

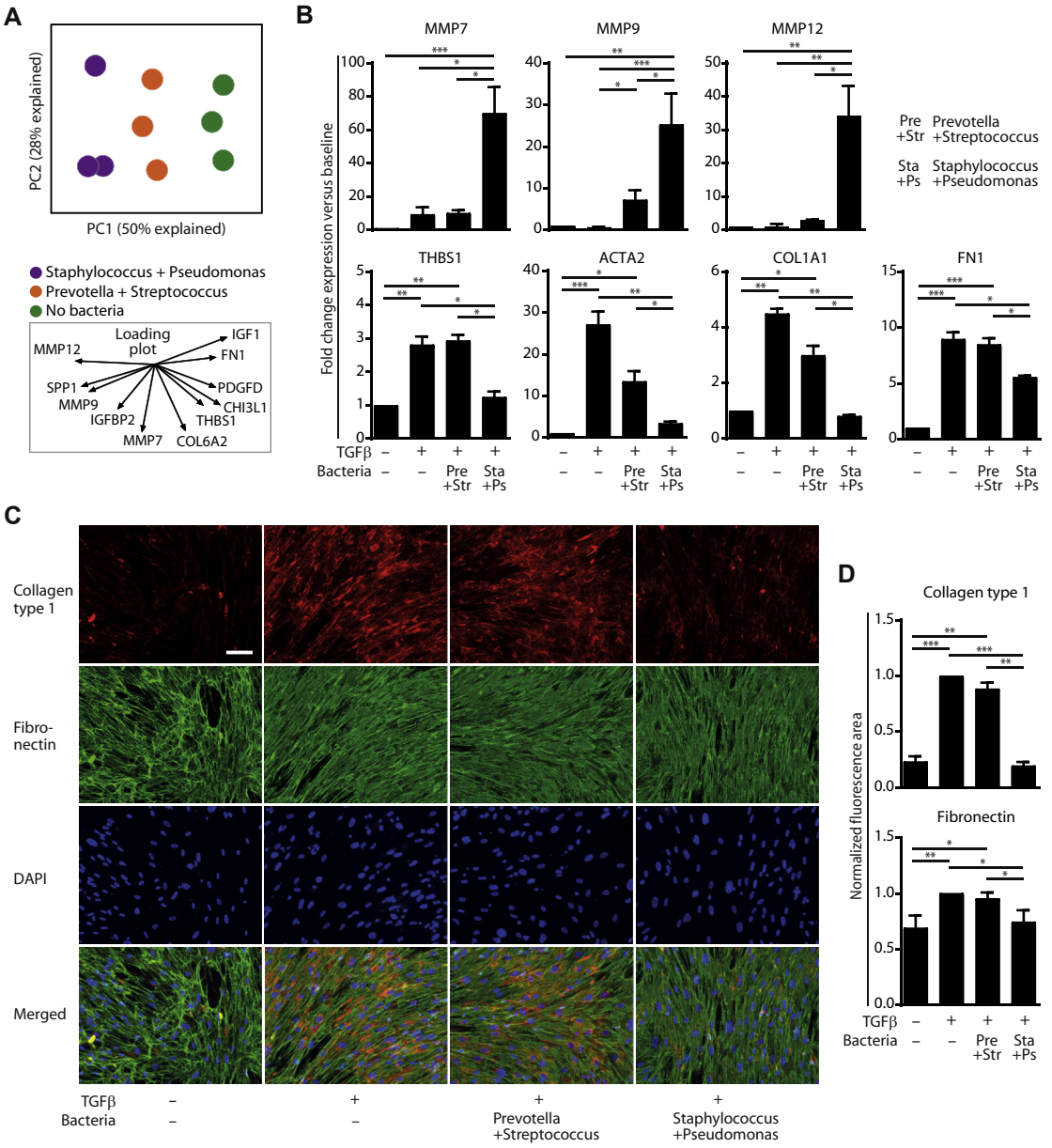

FIG 5. Impact of bacterial stimulation on remodeling gene expression in macrophage-fibroblast cocultures. **A,** Gene expression-based PC analysis. Dots represent the mean coordinates obtained from duplicates in 3 independent experiments. **B,** Quantitative PCR-based gene expression analysis. Immunostaining **(C)** and quantification **(D)** of deposited matrix proteins. Scale bar represents 100 μm. **B-D,** Data were from 6 independent experiments. Values represented as mean with SEM are expressed as fold-change over baseline. *$P < .05$, **$P < .01$, and ***$P < .001$.

gene expression profiles and matrix deposition. Culture conditions were optimized for efficient matrix deposition, and included immunosuppressive drugs, that mimicked the transplanted lung environment and antibiotics, which effectively prevented bacterial overgrowth (see the Methods for details). This ensured consistent cell viability levels across the different experimental conditions, in spite of a median 19% decrease in the presence of *S aureus* and *P aeruginosa* versus *P melaninogenica* and *S pneumoniae* (see Fig E2 in the Online Repository). In this setting, bacteria identified in lung transplant recipients on a catabolic remodeling background (a mix of *S aureus* and *P aeruginosa*) induced a globally distinct remodeling gene expression profile in macrophage-fibroblast cocultures, as compared to the representatives of the community linked to anabolic remodeling (*P melaninogenica* and *S pneumoniae*) (Fig 5, *A*). Specifically, *Staphylococcus* and *Pseudomonas* induced maximal expression of MMP7, -9, and -12, while *Prevotella* and *Streptococcus* were linked to higher THBS1 expression, 2 features aligning with catabolic and anabolic gene expression profiling in BAL cells of lung transplant recipients, respectively (Fig 5, *B*). *Staphylococcus* and *Pseudomonas* were more potent in repressing expression of the

marker of fibroblast to myofibroblast differentiation, α-smooth muscle actin, along with that of the matrix components collagen type 1 α1and fibronectin 1 (Fig 5, *B*). These divergent gene expression profiles were ultimately reflected by a marked decrease in matrix deposition linked to *Staphylococcus* and *Pseudomonas* versus *Prevotella* and *Streptococcus* exposure, as determined by collagen type 1 and fibronectin immunostaining (Fig 5, *C* and *D*).

Consequently, this dataset underscored the critical role of bacterial stimulation in the maintenance of homeostatic matrix turnover, suggesting that the detrimental impact of airway microbiota dysbiosis following transplantation may consist of exaggerated anabolic or catabolic remodeling processes.

DISCUSSION

The view of the lower airways representing an ecosystem implies that host cells and the constituents of the microbiota vary in a coordinated manner, particularly in the case of a breakdown in local homeostasis. Accordingly, different microbial communities have been observed in association with lung diseases such as asthma, chronic obstructive pulmonary disease (COPD), and idiopathic pulmonary fibrosis, versus the healthy state, with further changes prior, during, or following exacerbations.[4-6,23,24] The ecosystem associated with the transplanted lung is shaped by the early and continuous implementation of immunosuppression and the preventive or therapeutic use of antibiotics. We have previously reported that this lung habitat is linked to distinct microbial communities, which can influence macrophage gene expression.[7]

The present study aimed to discriminate between anabolic and catabolic remodeling following lung transplantation, given the contrasting implications for graft fate these mechanisms may have. In addition, we investigated the composition of lower airway microbial communities on the different remodeling backgrounds and addressed the impact of bacterial stimulation on remodeling using an *in vitro* system of matrix deposition.

The 11 remodeling-related target genes we selected have all previously been linked to respiratory conditions, though their pathological role remains elusive.[15,16,18,21,25-27] Functionally, the corresponding encoded factors can be divided in 4 main categories: (1) matrix structural constituents (collagen type VI α-2, fibronectin 1), which in myeloid cells are further known to modulate cell-matrix adhesion properties[18,28]; (2) matricellular proteins (THBS1, SPP1, CHI3L1, IGF binding protein 2), which comprise a variety of nonstructural, multifunctional factors, that transiently bind to the matrix under specific conditions, notably in association with lung injury, wound healing, and fibrogenesis[29]; (3) matrix metallopeptidases (MMP7, -9, -12) that fulfil multiple functions, but overall are associated with an enhanced matrix degradation or turnover; (4) growth factors (PDGFD, insulin-like growth factor 1), that regulate the proliferation, migration, and survival of key remodeling cell players.

Beside their implication in homeostatic matrix turnover, all of these factors are involved in the control of lung injury, where they function to ensure a time-dependent sequence of inflammatory and remodeling processes, which ultimately lead to tissue repair. Likewise, they have been linked to different respiratory conditions, where their production varies with disease progression. Hence, both the physiological and pathophysiological functions of these factors appear to be orchestrated in a time-dependent manner. In this respect, our study, supported by longitudinal data, shows marked differences in the kinetics of the 4 remodeling profiles identified following transplantation. Of particular interest, the frequency of the catabolic remodeling profile was maximal between 3 and 6 months, while the anabolic remodeling profile peaked between 12 and 24 months posttransplantation. Several factors associated with the catabolic remodeling profile have been linked to inflammatory and/or acute conditions, such as acute lung injury (SPP1),[30] severe asthma (CHI3L1),[31] or COPD exacerbation (CHI3L1).[25] Moreover, the upregulated production of MMPs by inflammatory, epithelial, and stromal cells, and the associated release in the lung and circulation of matrix degradation products, have been observed in a large panel of respiratory conditions, including CLAD versus stable lung transplant recipients.[32-35]

In contrast, THBS1 and PDGFD, 2 factors linked to the anabolic remodeling profile, have been reported to be part of a positive feedback loop with the prototypical profibrogenic factor TGF-β1, during tissue repair,[20,36] promoting fibroblast proliferation and myofibroblast differentiation.[36,37] Collectively, these observations suggest that the factors linked to the catabolic and anabolic remodeling profiles identified are active in distinct remodeling processes and/or stages.

The lower airway microbiota composition also varies over time posttransplantation. We observed that a maximal frequency of communities, strongly dominated by highly stimulatory bacteria (from 3 to 6 months), coincided both with the peak of bacterial infection and that of the catabolic remodeling profile. In marked contrast, the maximal frequency of communities dominated by low stimulatory bacteria (from 12 months onward), aligned with the kinetics of the anabolic remodeling profile, suggesting that the interplay among host cells, microbes, and the matrix represents a key determinant of the lower airway microenvironment. In this respect, data suggest that increases in BAL and/or circulating matrix degradation products coincide with shifts in airway microbiota composition during exacerbations in COPD and idiopathic pulmonary fibrosis.[5,6,34,38] Furthermore, matricellular proteins play important roles in innate immune mechanisms linked to both physiological bacterial colonization and infection, such as the regulation of bioactive antibacterial peptide release.[39,40]

Our *in vitro* dataset indicates that *S aureus* and *P aeruginosa*, typically associated with proinflammatory microbial communities, trigger a stronger catabolic remodeling profile, in comparison to *P melaninogenica* and *S pneumoniae*. This is consistent with recent observations linking the 2 former bacterial species to increased BAL levels of matrix glycosaminoglycans, as compared to those associated with *S pneumoniae*, in acute exacerbation and stable COPD, respectively.[41] There are different ways bacteria could modulate matrix production in our *in vitro* system. Fig 5, *A-D* indicates that this occurred through stimulation of fibroblasts and macrophages, by shifting the gene expression balance between matrix components and metalloproteinases. In addition, bacteria could have impacted remodeling through direct degradation of the matrix. However, given the presence of antibiotics in the culture medium, which efficiently prevented bacterial metabolic activities, this second mode of action is likely to be insignificant in this setting. Consequently, we propose that the observed effects are linked to the higher stimulatory potential of the microbe-associated molecular patterns, such as peptidoglycan and lipopolysaccharide,

which contribute to the structural properties of bacterial cells in *Staphylococcus* and *Pseudomonas* versus those in *Prevotella* and *Streptococcus*. Regardless of the mechanisms involved, these observations suggest that the net effect of host-microbe interactions on matrix regulation closely depends on the microbiota constituents. We propose that in the healthy state, the lower airway microenvironmental conditions are linked to low-grade matrix turnover and a balanced microbiota, which contribute to local homeostasis. However, in respiratory diseases associated with acute inflammation or fibrogenesis, local conditions linked to a catabolic and anabolic remodeling profile, respectively, promote the growth of specific bacteria, which in turn differentially impact matrix regulation.

There were limitations to this study. First, although our *in vitro* dataset revealed a link between remodeling gene expression levels and activities, we acknowledge that remodeling in the transplanted lung cannot be inferred solely from the identification of BAL cell gene expression profiles, given the importance of posttranscriptional regulation in this process. Nonetheless, the different remodeling gene expression profiles we identified correspond to distinct microenvironmental conditions, as corroborated by specific features in the lung microbiota composition and the underlying clinical state. Second, while the anabolic and catabolic remodeling profiles distinguished 2 well-delineated sample groups, as further confirmed by their association with contrasting bacterial communities, we found no such associations for the low and intermediate remodeling profiles. A possible underlying reason is that these 2 latter profiles reflect local conditions that are convergent enough to accommodate similar microbial communities. Alternatively, the analytical tools we used to characterize gene expression profiling and the composition of the airway microbiota might not have reached the power required to further dissect existing associations. Third, given that remodeling gene expression was measured from unsorted BAL cells, we could not ascertain the cellular source of gene transcripts, which would provide information about the underlying pathophysiological processes. Fourth, the posttransplantation follow-up period was not long enough to enable us to assess any distinction between stable transplant recipients and patients with CLAD. Given the progressive nature and prevalence of this major obstacle to long-term graft survival, further studies with a minimal 3-year longitudinal follow-up are required to elucidate a link between pulmonary bacterial dysbiosis, host gene expression profiling, and eventually pathophysiological tissue remodeling. Fifth, a direct assessment of the impact of antibiotics and immunosuppressive drugs was precluded by the broad use, large variability, and partly overlapping effects of the applied regimens, within the context of lung transplantation. Sixth, a full picture of the airway ecosystem should include an in-depth characterization of the viral and fungal microbiota constituents. Notwithstanding these shortcomings, our collective findings shed light on the role of host-microbe interactions in the control of matrix turnover after lung transplantation. Further increasing our understanding of the mechanisms implicated may help decipher the pathophysiology of CLAD and, by inference, that of other respiratory conditions associated with lower airway remodeling.

We thank M.-F. Derkenne, B. Camara, C. Chérion, J. Stauder, S. Ali-Azouaou, T. Rechsteiner, and C. Cowaloosur-Noirat for their contribution in sample collection and clinical data management; A. Rapin for assistance in 16S rRNA gene Illumina sequencing; and J. Pernot for technical assistance.

Key messages

- **Four host remodeling gene expression profiles that align with different bacterial communities prevail in the transplanted lung.**
- **Typical bacterial pathogens that occasionally bloom during the first months posttransplantation appear to promote the degradation of the extracellular matrix, while bacteria belonging to a healthy steady-state microbiota permit fibroblast to myofibroblast differentiation and matrix deposition.**

REFERENCES

1. Yusen RD, Edwards LB, Kucheryavaya AY, Benden C, Dipchand AI, Goldfarb SB, et al. The Registry of the International Society for Heart and Lung Transplantation: Thirty-second Official Adult Lung and Heart-Lung Transplantation Report–2015; Focus Theme: Early Graft Failure. J Heart Lung Transplant 2015;34:1264-77.
2. Suwara MI, Vanaudenaerde BM, Verleden SE, Vos R, Green NJ, Ward C, et al. Mechanistic differences between phenotypes of chronic lung allograft dysfunction after lung transplantation. Transpl Int 2014;27:857-67.
3. Charlson ES, Diamond JM, Bittinger K, Fitzgerald AS, Yadav A, Haas AR, et al. Lung-enriched organisms and aberrant bacterial and fungal respiratory microbiota after lung transplant. Am J Respir Crit Care Med 2012;186:536-45.
4. Hilty M, Burke C, Pedro H, Cardenas P, Bush A, Bossley C, et al. Disordered microbial communities in asthmatic airways. PLoS One 2010;5:e8578.
5. Huang YJ, Sethi S, Murphy T, Nariya S, Boushey HA, Lynch SV. Airway microbiome dynamics in exacerbations of chronic obstructive pulmonary disease. J Clin Microbiol 2014;52:2813-23.
6. Molyneaux PL, Cox MJ, Willis-Owen SA, Mallia P, Russell KE, Russell AM, et al. The role of bacteria in the pathogenesis and progression of idiopathic pulmonary fibrosis. Am J Respir Crit Care Med 2014;190:906-13.
7. Bernasconi E, Pattaroni C, Koutsokera A, Pison C, Kessler R, Benden C, et al. Airway microbiota determines innate cell inflammatory or tissue remodeling profiles in lung transplantation. Am J Respir Crit Care Med 2016;194:1252-63.
8. Pison C, Magnan A, Botturi K, Sève M, Brouard S, Marsland BJ, et al. Prediction of chronic lung allograft dysfunction: a systems medicine challenge. Eur Respir J 2014;43:689-93.
9. Stewart S, Fishbein MC, Snell GI, Berry GJ, Boehler A, Burke MM, et al. Revision of the 1996 working formulation for the standardization of nomenclature in the diagnosis of lung rejection. J Heart Lung Transplant 2007;26:1229-42.
10. Carbon S, Ireland A, Mungall CJ, Shu S, Marshall B, Lewis S, et al. AmiGO: online access to ontology and annotation data. Bioinformatics 2009;25:288-9.
11. Yadava K, Pattaroni C, Sichelstiel AK, Trompette A, Gollwitzer ES, Salami O, et al. Microbiota promotes chronic pulmonary inflammation by enhancing IL-17A and autoantibodies. Am J Respir Crit Care Med 2016;193:975-87.
12. Langille MG, Zaneveld J, Caporaso JG, McDonald D, Knights D, Reyes JA, et al. Predictive functional profiling of microbial communities using 16S rRNA marker gene sequences. Nat Biotechnol 2013;31:814-21.
13. Team RDC. R: A language and environment for statistical computing. Vienna, Austria: R Foundation for Statistical Computing; 2011.
14. Cao B, Guo Z, Zhu Y, Xu W. The potential role of PDGF, IGF-1, TGF-beta expression in idiopathic pulmonary fibrosis. Chin Med J (Engl) 2000;113:776-82.
15. Guiot J, Bondue B, Henket M, Corhay JL, Louis R. Raised serum levels of IGFBP-1 and IGFBP-2 in idiopathic pulmonary fibrosis. BMC Pulm Med 2016;16:86.
16. Ide M, Ishii H, Mukae H, Iwata A, Sakamoto N, Kadota J, et al. High serum levels of thrombospondin-1 in patients with idiopathic interstitial pneumonia. Respir Med 2008;102:1625-30.
17. Jonigk D, Izykowski N, Rische J, Braubach P, Kuhnel M, Warnecke G, et al. Molecular profiling in lung biopsies of human pulmonary allografts to predict chronic lung allograft dysfunction. Am J Pathol 2015;185:3178-88.
18. Pardo A, Gibson K, Cisneros J, Richards TJ, Yang Y, Becerril C, et al. Up-regulation and profibrotic role of osteopontin in human idiopathic pulmonary fibrosis. PLoS Med 2005;2:e251.

19. Schnoor M, Cullen P, Lorkowski J, Stolle K, Robenek H, Troyer D, et al. Production of type VI collagen by human macrophages: a new dimension in macrophage functional heterogeneity. J Immunol 2008;180:5707-19.
20. Sweetwyne MT, Murphy-Ullrich JE. Thrombospondin1 in tissue repair and fibrosis: TGF-beta-dependent and independent mechanisms. Matrix Biol 2012; 31:178-86.
21. Taylor SL, Rogers GB, Chen AC, Burr LD, McGuckin MA, Serisier DJ. Matrix metalloproteinases vary with airway microbiota composition and lung function in non-cystic fibrosis bronchiectasis. Ann Am Thorac Soc 2015;12:701-7.
22. Zhuo Y, Zhang J, Laboy M, Lasky JA. Modulation of PDGF-C and PDGF-D expression during bleomycin-induced lung fibrosis. Am J Physiol Lung Cell Mol Physiol 2004;286:L182-8.
23. Larsen JM, Musavian HS, Butt TM, Ingvorsen C, Thysen AH, Brix S. Chronic obstructive pulmonary disease and asthma-associated Proteobacteria, but not commensal Prevotella spp., promote Toll-like receptor 2-independent lung inflammation and pathology. Immunology 2015;144:333-42.
24. Dickson RP, Martinez FJ, Huffnagle GB. The role of the microbiome in exacerbations of chronic lung diseases. Lancet 2014;384:691-702.
25. Lai T, Wu D, Chen M, Cao C, Jing Z, Huang L, et al. YKL-40 expression in chronic obstructive pulmonary disease: relation to acute exacerbations and airway remodeling. Respir Res 2016;17:31.
26. Uh ST, Inoue Y, King TE Jr, Chan ED, Newman LS, Riches DW. Morphometric analysis of insulin-like growth factor-I localization in lung tissues of patients with idiopathic pulmonary fibrosis. Am J Respir Crit Care Med 1998; 158:1626-35.
27. Zhou Y, Peng H, Sun H, Peng X, Tang C, Gan Y, et al. Chitinase 3-like 1 suppresses injury and promotes fibroproliferative responses in Mammalian lung fibrosis. Sci Transl Med 2014;6:240ra76.
28. Gratchev A, Guillot P, Hakiy N, Politz O, Orfanos CE, Schledzewski K, et al. Alternatively activated macrophages differentially express fibronectin and its splice variants and the extracellular matrix protein betaIG-H3. Scand J Immunol 2001;53: 386-92.
29. Murphy-Ullrich JE, Sage EH. Revisiting the matricellular concept. Matrix Biol 2014;37:1-14.
30. Wang KX, Denhardt DT. Osteopontin: role in immune regulation and stress responses. Cytokine Growth Factor Rev 2008;19:333-45.
31. Chupp GL, Lee CG, Jarjour N, Shim YM, Holm CT, He S, et al. A chitinase-like protein in the lung and circulation of patients with severe asthma. N Engl J Med 2007;357:2016-27.
32. Kristensen JH, Larsen L, Dasgupta B, Brodmerkel C, Curran M, Karsdal MA, et al. Levels of circulating MMP-7 degraded elastin are elevated in pulmonary disorders. Clin Biochem 2015;48:1083-8.
33. Pain M, Royer P-J, Loy J, Girardeau A, Tissot A, Lacoste P, et al. T cells promote bronchial epithelial cells secretion of matrix-metalloproteinase-9 via a C-C chemokine receptor type 2 pathway, implications for chronic lung allograft dysfunction. Am J Transplant 2017;17:1502-14.
34. Stolz D, Leeming DJ, Kristensen JH, Karsdal MA, Boersma W, Louis R, et al. Systemic biomarkers of collagen and elastin turnover are associated with clinically relevant outcomes in COPD. Chest 2017;151:47-59.
35. Vandermeulen E, Verleden SE, Bellon H, Ruttens D, Lammertyn E, Claes S, et al. Humoral immunity in phenotypes of chronic lung allograft dysfunction: a broncho-alveolar lavage fluid analysis. Transpl Immunol 2016;38:27-32.
36. Zhao T, Zhao W, Chen Y, Li VS, Meng W, Sun Y. Platelet-derived growth factor-D promotes fibrogenesis of cardiac fibroblasts. Am J Physiol Heart Circ Physiol 2013;304:H1719-26.
37. Buhl EM, Djudjaj S, Babickova J, Klinkhammer BM, Folestad E, Borkham-Kamphorst E, et al. The role of PDGF-D in healthy and fibrotic kidneys. Kidney Int 2016;89:848-61.
38. Jenkins RG, Simpson JK, Saini G, Bentley JH, Russell AM, Braybrooke R, et al. Longitudinal change in collagen degradation biomarkers in idiopathic pulmonary fibrosis: an analysis from the prospective, multicentre PROFILE study. Lancet Respir Med 2015;3:462-72.
39. Dela Cruz CS, Liu W, He CH, Jacoby A, Gornitzky A, Ma B, et al. Chitinase 3-like-1 promotes Streptococcus pneumoniae killing and augments host tolerance to lung antibacterial responses. Cell Host Microbe 2012;12: 34-46.
40. Gela A, Bhongir RK, Mori M, Keenan P, Morgelin M, Erjefalt JS, et al. Osteopontin that is elevated in the airways during COPD impairs the antibacterial activity of common innate antibiotics. PLoS One 2016;11:e0146192.
41. Papakonstantinou E, Klagas I, Roth M, Tamm M, Stolz D. Acute exacerbations of COPD are associated with increased expression of heparan sulfate and chondroitin sulfate in BAL. Chest 2016;149:685-95.

LIST OF SysCLAD CONSORTIUM MEMBERS

Cohort of Lung Transplantation (COLT) (Surgeons; Anesthetists-Intensivists; Physicians; Research staff)

Bordeaux: J. Jougon, J.-F. Velly; H. Rozé; E. Blanchard, C. Dromer.

Brussels: M. Antoine, M. Cappello, M. Ruiz, Y. Sokolow, F. Vanden Eynden, G. Van Nooten; L. Barvais, J. Berré, S. Brimioulle, D. De Backer, J. Créteur, E. Engelman, I. Huybrechts, B. Ickx, T. J. C. Preiser, T. Tuna, L. Van Obberghe, N. Vancutsem, J.-L. Vincent; P. De Vuyst, I. Etienne, F. Féry, F. Jacobs, C. Knoop, J. L. Vachiéry, P. Van den Borne, I. Wellemans; G. Amand, L. Collignon, M. Giroux.

Grenoble: D. Angelescu, O. Chavanon, R. Hacini, A. Pirvu, P. Porcu; P. Albaladejo, C. Allègre, A. Bataillard, D. Bedague, E. Briot, M. Casez-Brasseur, D. Colas, G. Dessertaine, M. Durand, G. Francony, A. Hebrard, M. R. Marino, B. Oummahan, D. Protar, D. Rehm, S. Robin, M. Rossi-Blancher; C. Augier, P. Bedouch, A. Boignard, H. Bouvaist, A. Briault, B. Camara, J. Claustre, S. Chanoine, M. Dubuc, S. Quétant, J. Maurizi, P. Pavèse, C. Pison, C. Saint-Raymond, N. Wion; C. Chérion.

Lyon: R. Grima, O. Jegaden, J.-M. Maury, F. Tronc, C. Flamens, S. Paulus; J.-F. Mornex, F. Philit, A. Senechal, J.-C. Glérant, S. Turquier; D. Gamondes, L. Chalabresse, F. Thivolet-Bejui; C. Barnel, C. Dubois, A. Tiberghien.

Paris, Hôpital Européen Georges Pompidou: F. Le Pimpec-Barthes, A. Bel, P. Mordant, P. Achouh; V. Boussaud; R. Guillemain, D. Méléard, M. O. Bricourt, B. Cholley; V. Pezella.

Marseille: G. Brioude, X. B. D'Journo, C. Doddoli, P. Thomas, D. Trousse; S. Dizier, M. Leone, L. Papazian, F. Bregeon; A. Basire, B. Coltey, N. Dufeu, H. Dutau, S. Garcia, J. Y. Gaubert, C. Gomez, S. Laroumagne, A. Nieves, L. C. Picard, M. Reynaud-Gaubert; V. Secq, G. Mouton.

Nantes: O. Baron, P. Lacoste, C. Perigaud, J. C. Roussel; I. Danner, A. Haloun, A. Magnan, A. Tissot; T. Lepoivre, M. Treilhaud; K. Botturi-Cavaillès, S. Brouard, R. Danger, J. Loy, M. Morisset, M. Pain, S. Pares, D. Reboulleau, P.-J. Royer.

Le Plessis Robinson, Hôpital Marie Lannelongue: D. Fabre, E. Fadel, O. Mercier, S. Mussot; F. Stephan, P. Viard; J. Cerrina, P. Dorfmuller, S. M. Ghigna, Ph. Hervén, F. Le Roy Ladurie, J. Le Pavec, V. Thomas de Montpreville; L. Lamrani.

Paris, Hôpital Bichat: Y. Castier, P. Mordant, P. Cerceau, P. Augustin, S. Jean-Baptiste, S. Boudinet, P. Montravers; O. Brugière, G. Dauriat, G. Jébrak, H. Mal, A. Marceau, A.-C. Métivier, G. Thabut, E. Lhuillier, C. Dupin, V. Bunel.

Strasbourg: P. Falcoz, G. Massard, N. Santelmo; G. Ajob, O. Collange O. Helms, J. Hentz, A. Roche; B. Bakouboula, T. Degot, A. Dory, S. Hirschi, S. Ohlmann-Caillard, L. Kessler, R. Kessler, A. Schuller; K. Bennedif, S. Vargas, J. Stauder, S. Ali-Azouaou.

Suresnes: P. Bonnette, A. Chapelier, P. Puyo, E. Sage, J. Bresson, V. Caille, C. Cerf, J. Devaquet, V. Dumans-Nizard, M.-L. Felten, M. Fischler, A.-G. Si Larbi, M. Leguen, L. Ley, N. Liu, G. Trebbia; S. De Miranda, B. Douvry, F. Gonin, D. Grenet, A. M. Hamid, H. Neveu, F. Parquin, C. Picard, A. Roux, M. Stern; F. Bouillioud, P. Cahen, M. Colombat, C. Dautricourt, M. Delahousse, B. D'Urso, J. Gravisse, A. Guth, S. Hillaire, P. Honderlick, M. Lequintrec, E. Longchampt, F. Mellot, A. Scherrer, L. Temagoult, L. Tricot; M. Vasse, C. Veyrie, L. Zemoura.

Toulouse: J. Berjaud, L. Brouchet, M. Dahan; F. O. Mathe; H. Benahoua, M. DaCosta, I. Serres, V. Merlet-Dupuy, M. Grigoli, A. Didier, M. Murris; L. Crognier, O. Fourcade.

Swiss Transplant Cohort Study (STCS)

Lausanne: T. Krueger, H. B. Ris, M. Gonzalez, Ph. Jolliet, C. Marcucci, M. Chollet, F. Gronchi, C. Courbon, C. Berutto, O. Manuel, A. Koutsokera, J.-D. Aubert, L. P. Nicod, S. Mouraux, E. Bernasconi, C. Pattaroni, B. J. Marsland.

Geneva: P. M. Soccal, T. Rochat, L. M. Lücker.

Zurich: S. Hillinger, I. Inci, W. Weder, R. Schuepbach, M. Zalunardo, C. Benden, M. M. Schuurmans, A. Gaspert, D. Holzmann, N. Müller, C. Schmid, B. Vrugt.

Small and Medium-sized Enterprises, and platforms

Biomax, Planegg, Germany: A. Fritz, D. Maier.

Finovatis, Lyon, France: K. Deplanche, D. Koubi.

GATC Biotech, Konstanz, Germany: F. Ernst, T. Paprotka, M. Schmitt, B. Wahl.

Novasdicovery, Lyon, France: J.-P. Boissel, G. Olivera-Botello.

Prométhée Proteomics Platform, Grenoble, France: C. Trocmé, B. Toussaint, S. Bourgoin-Voillard, M. Sève.

Institut National de la Santé et de la Recherche Médicale U823, Université Grenoble Alpes, Grenoble, France: M. Benmerad, V. Siroux, R. Slama.

European Institute for Systems Biology and Medicine, Lyon, France: C. Auffray, D. Charron, D. Lefaudeux, J. Pellet.

METHODS

Patient sample collection

Patients underwent transoral or transnasal bronchoscopy. For BAL fluid (BALF) collection, the bronchoscope was wedged either in the middle lobe or lingula of the allograft and 100 to 150 mL of normal saline were instilled. Different fractions of collected samples were submitted to cell differential determination, culture-dependent bacterial and fungal detection, and PCR-based detection of viral infection, according to routine clinical procedures. Two fractions of 3 mL were stored at 4°C and centrifuged within 3 hours at either 2,000*g* or 14,000*g* for 10 minutes, for future isolation of BALF cellular RNA and total DNA, respectively. Pellets were snap frozen, either after cell lysis in RLT buffer (Qiagen, Hilden, Germany) to preserve RNA integrity, or directly, and were stored at −80°C until further processing. Samples obtained on washing the endoscope with sterile saline prior an examination were prepared following the same procedure and were used as negative control samples.

BALF cellular RNA extraction and real-time quantitative PCR for gene expression analysis

BALF cell lysates were transferred into a QIAshredder column (Qiagen) for homogenization and total RNA was extracted using RNeasy Mini Kit (Qiagen) according to the manufacturer's instructions. RNA concentration was determined using a Nanodrop ND-1000 spectrophotometer (Thermo Fisher Scientific, Waltham, Mass) and reverse transcription was performed using iScript cDNA Synthesis Kit (Bio-Rad, Hercules, Calif). Characterization of BALF cell remodeling profiles was based on multiplex real-time PCR analysis of expression of a set of 11 genes (Table II). We used guanine nucleotide-binding protein, β-polypeptide 2-like 1 gene as a reference gene, given its high expression stability in BALF cells in both health and disease.[E1] Custom oligonucleotide primers and probes (Table E1) were designed using National Center for Biotechnology Information (Bethesda, Md) primer blast software and were purchased from Microsynth (Balgach,

Switzerland). Amplification was carried out using iQ Multiplex Powermix and a CFX96 Real-Time detection system. Absolute quantification was performed using the CFX Manager software 2.1 (all from Bio-Rad) based on values obtained with a set of purified amplicons used as standards.

Bacterial metagenome prediction

The operational taxonomic units table obtained from 16S rRNA gene sequencing data was normalized relative to the 16S rRNA gene copy number, and the metagenomic content was predicted using PICRUSt software. The predicted metagenome was exported as KOs for principal coordinate analysis on Bray-Curtis distance, using the cmdscale function in R. To investigate the potential functional capacity of the bacterial metagenome in respect to host remodeling, a subset of 159 KOs related to matrix interactions (search terms chondroitin*, collagen*, fibrinogen, fibronectin, hyaluron*) or protein/peptide degradation (search terms protease, proteinase, peptidase, *lysin, *pain, *staphin) were selected. All of these KOs were previously reported to be linked to bacterial genomes.

Bacterial cultures

Staphylococcus aureus (ATCC 25904) and *P aeruginosa* (ATCC BAA-47) were cultured on tryptic soy agar or in tryptic soy broth at 37°C with 130 and 200 revolutions/min agitation, respectively (all media were obtained from Becton-Dickinson, Franklin Lakes, NJ, unless otherwise specified). *Streptococcus pneumoniae* (NCTC 7466) was grown on Mueller Hinton agar with 5% sheep blood or in tryptic soy broth at 37°C, in absence of agitation in a 5% CO2 incubator. *Prevotella melaninogenica* (ATCC 25845) was cultured on Columbia agar with 5% sheep blood or in chopped meat broth (Remel Laboratories, Lenexa, Kan) at 37°C under anaerobic conditions. For stimulation experiments, bacteria were grown for 16 hours, washed twice in PBS (BioConcept, Allschwil, Switzerland) at 3000*g* for 10 minutes at 4°C, and resuspended in X-VIVO 15 medium (Lonza, Basel, Switzerland). Suspensions were finally diluted to reach a concentration of 4×10^{-3} (*P aeruginosa* and *S pneumoniae*) or 2×10^{-3} (*S aureus* and *P melaninogenica*) optical density at 600 nm corresponding to 10^6 CFU/mL.

In vitro macrophage-fibroblast maintenance and stimulation experiments

The MRC-5 (ATCC CCL-171) human fibroblast cell line was maintained in minimum essential medium with Earle's salts, supplemented with nonessential amino acids, sodium pyruvate, 10% (vol/vol) heat inactivated FBS and 100 U/mL penicillin and 100 μg/mL streptomycin (all from Thermo Fisher Scientific). The THP-1 (ATCC TIB-202) human monocytic cell line was maintained in RPMI 1640 medium supplemented with 10% (vol/vol) heat inactivated FBS, 20 μmol/L 2-mercaptoethanol, 100 U/mL penicillin, and 100 μg/mL streptomycin (all from Thermo Fisher Scientific). Incubation was at 37°C in a humidified 5% CO_2 atmosphere. For generating THP-DM, 24-well plates were precoated with FBS for 60 minutes. THP1 cells were centrifuged at 300*g* for 10 minutes, resuspended in differentiation medium, which corresponded to maintenance medium supplemented with human recombinant Macrophage-Colony Stimulating Factor (Peprotech, Rocky Hill, NJ), FBS (20% final concentration) and 10 mmol/L HEPES, and were seeded into precoated 24-well plates at a density of 10^5 cells per well. Incubation was for 7 days, without medium change. To assess gene expression levels in macrophage-fibroblast cocultures in the presence or absence of bacteria, fibroblasts and THP-DM were seeded at a density of 40,000 and 20,000 cells/cm^2, respectively, in serum-free minimum essential medium with Earle's salts containing TGF-β1 (5 ng/mL; eBioscience, San Diego, Calif), a mixture of prednisolone (500 nmol/L; Sigma, St. Louis, Mo)/FK506 (tacrolimus, 25 nmol/L; Enzo Life Sciences, Lausen, Switzerland)/mycophenolic acid (10 μmol/L; Tocris Bioscience, Ellisville, Mo), and penicillin and streptomycin (1000 U/mL and 100 μg/mL, respectively; Thermo Fisher Scientific). Bacterial suspensions were added 16 hours postseeding, at a total density of 3×10^5 CFU/cm^2, which corresponded to 5 CFU per eukaryotic cell at day 0, and the effects of stimulation were assessed 30 hours later, when supernatants were removed and cells were lyzed in RLT buffer (Qiagen) to preserve RNA integrity. Cell viability was assessed 30 hours following the addition of bacterial mixtures into macrophage-fibroblast cocultures, using a WST-1-based colorimetric assay (Cell Counting Kit-8, Dojindo Molecular Technologies, Rockville, Md), according to the manufacturer's instructions.

In vitro assessment of matrix deposition

To optimize for maximal matrix deposition, macrophage-fibroblast coculture medium was supplemented with 70- and 400-kDa Ficoll (37.5 and 25 mg/mL, respectively; GE Healthcare, Little Chalfont, UK).[E2] Cocultures were seeded at a density of 25,000 and 12,500 cells/cm^2, respectively, in μ-Slide 8-well ibi-Treat slides (Ibidi, Martinsried, Germany), and were incubated for 6 days without medium change, in the presence or absence of bacteria, and thereafter supernatants were removed and cells were fixed in 4% paraformaldehyde in PBS for 20 minutes, for subsequent immunostaining analysis.

Immunostaining, image acquisition, and measurement of fluorescence area

Paraformaldehyde-fixed cells were permeabilized for 10 minutes in 0.2% Triton X-100 in PBS, and further incubated for 30 minutes in 1% BSA (Sigma-Aldrich, St Louis, Mo) in PBS to reduce nonspecific antibody binding. Primary antibodies (mouse anti-human collagen type 1, Sigma-Aldrich; and rabbit anti-human fibronectin, Abcam, Cambridge, UK) and secondary antibodies (goat anti-mouse IgG Cy3, Merck, Darmstadt, Germany; and goat anti-rabbit IgG AlexaFluor 488, Thermo Fisher Scientific) were incubated for 2 hours and 1 hour, respectively, in 1% BSA in PBS. Incubation with 4′,6-diamidino-2-phenylindole dihydrochloride (10 μg/mL in methanol; PanReac AppliChem, Darmstadt, Germany) was for 15 minutes. All steps were performed at room temperature. For image acquisition, we used a motorized inverted fluorescence microscope (Axio Observer Z1, Carl Zeiss, Oberkochen, Germany) with 20× objective. A consistent predetermined pattern of 8 images were acquired, both within and across experiments. The process was automated using the Mark&Find function in AxioVision imaging software (release 4.7.1, Carl Zeiss MicroImaging, Goettingen, Germany). The fluorescence area was quantified and cell nuclei were counted with ImageJ (version 1.50b) software (National Institutes of Health, Bethesda, Md).

REFERENCES

E1. Ishii T, Wallace AM, Zhang X, Gosselink J, Abboud RT, English JC, et al. Stability of housekeeping genes in alveolar macrophages from COPD patients. Eur Respir J 2006;27:300-6.

E2. Kumar P, Satyam A, Fan X, Collin E, Rochev Y, Rodriguez BJ, et al. Macromolecularly crowded in vitro microenvironments accelerate the production of extracellular matrix-rich supramolecular assemblies. Sci Rep 2015;5:8729.

E3. Stewart S, Fishbein MC, Snell GI, Berry GJ, Boehler A, Burke MM, et al. Revision of the 1996 working formulation for the standardization of nomenclature in the diagnosis of lung rejection. J Heart Lung Transplant 2007;26:1229-42.

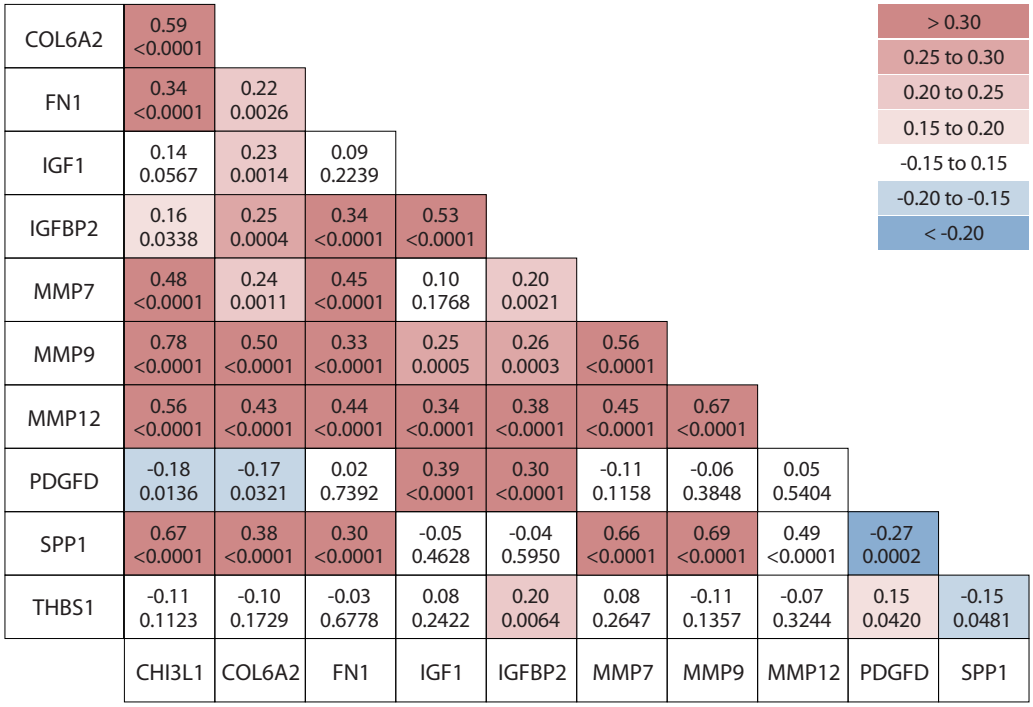

	CHI3L1	COL6A2	FN1	IGF1	IGFBP2	MMP7	MMP9	MMP12	PDGFD	SPP1
COL6A2	0.59 <0.0001									
FN1	0.34 <0.0001	0.22 0.0026								
IGF1	0.14 0.0567	0.23 0.0014	0.09 0.2239							
IGFBP2	0.16 0.0338	0.25 0.0004	0.34 <0.0001	0.53 <0.0001						
MMP7	0.48 <0.0001	0.24 0.0011	0.45 <0.0001	0.10 0.1768	0.20 0.0021					
MMP9	0.78 <0.0001	0.50 <0.0001	0.33 <0.0001	0.25 0.0005	0.26 0.0003	0.56 <0.0001				
MMP12	0.56 <0.0001	0.43 <0.0001	0.44 <0.0001	0.34 <0.0001	0.38 <0.0001	0.45 <0.0001	0.67 <0.0001			
PDGFD	-0.18 0.0136	-0.17 0.0321	0.02 0.7392	0.39 <0.0001	0.30 <0.0001	-0.11 0.1158	-0.06 0.3848	0.05 0.5404		
SPP1	0.67 <0.0001	0.38 <0.0001	0.30 <0.0001	-0.05 0.4628	-0.04 0.5950	0.66 <0.0001	0.69 <0.0001	0.49 <0.0001	-0.27 0.0002	
THBS1	-0.11 0.1123	-0.10 0.1729	-0.03 0.6778	0.08 0.2422	0.20 0.0064	0.08 0.2647	-0.11 0.1357	-0.07 0.3244	0.15 0.0420	-0.15 0.0481

FIG E1. Spearman correlation coefficient matrix based on expression levels of the selected 11 remodeling genes. Gene names are listed in Table II. Data are presented as Spearman ρ with *P* value, obtained by analyzing by quantitative PCR expression of the 11 selected genes in the total set of 187 BAL samples.

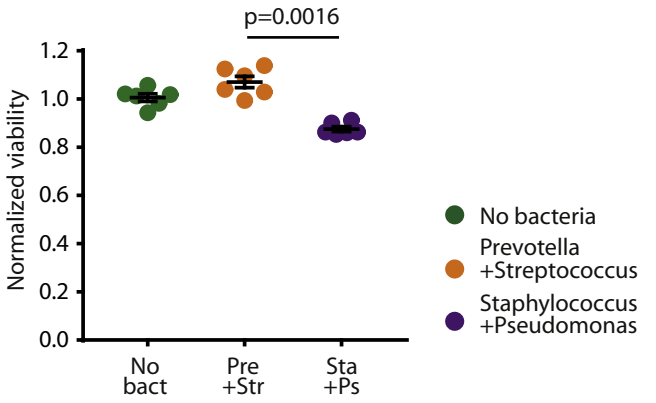

FIG E2. Cell viability determined in fibroblast-THP-DM cocultures, either in the absence (no bacteria) or presence of bacterial mixtures, as indicated. Data were pooled from 3 independent experiments with duplicates. Values (mean ± SEM) were normalized to viability levels in the absence of bacteria. Statistical significance was determined using Friedman test and Dunn *post hoc* analysis.

TABLE E1. Oligonucleotide primers and probes for analysis of BAL cell profiling

Oligonucleotide name	NCBI gene ID	NCBI reference sequence	5′ label	Sequence
CHI3L1_forward			—	5′-GATTTTCATGGAGCCTGGCG-3′
CHI3L1_reverse	1116	NM_001276.2	—	5′-CCCCACAGCATAGTCAGTGTT-3′
CHI3L1_probe			Tx Red	5′-ACAGGCCATCACAGTCCCCTGTTCCGA-3′
COL6A2_forward			—	5′-AGCTCTACCGCAACGACTAC-3′
COL6A2_reverse	1292	NM_001849.3	—	5′-CACCTTGTAGCACTCTCCGT-3′
COL6A2_probe			FAM	5′-ACTCCACCGAGATCGACCAGGACACCA-3′
MMP7_forward			—	5′-AAGTGGTCACCTACAGGATCG-3′
MMP7_reverse	4316	NM_002423.4	—	5′-TCAGCAGTTCCCCATACAACT-3′
MMP7_probe			Cy5	5′-ACATGTGGGGCAAAGAGATCCCCCTGC-3′
MMP9_forward			—	5′-GTACTCGACCTGTACCAGCG-3′
MMP9_reverse	4318	NM_004994.2	—	5′-AACAAACTGTATCCTTGGTCCG-3′
MMP9_probe			HEX	5′-ACAGCGACAAGAAGTGGGGCTTCTGCC-3′
IGF1_forward			—	5′-GCTTTTATTTCAACAAGCCCACAG-3′
IGF1_reverse	3479	NM_001111283.2	—	5′-GCCTCCTTAGATCACAGCTCC-3′
IGF1_probe			HEX	5′-ACAGGCATCGTGGATGAGTGCTGCTTCC-3′
IGFBP2_forward				5′-AACCTCAAACAGTGCAAGATGTC-3′
IGFBP2_reverse	3485	NM_000597.2		5′-GTAGAAGAGATGACACTCGGGG-3′
IGFBP2_probe			Tx Red	5′-AGCGTGGGGAGTGCTGGTGTGTGAA-3′
SPP1_forward				5′-TAAATTCTGGGAGGGCTTGGTT-3′
SPP1_reverse	6696	NM_001040060.1		5′-CATGGTAGTGAGTTTTCCTTGGTC-3′
SPP1_ probe			Cy5	5′-AGGCCAGTTGCAGCCTTCTCAGCCA-3′
THBS1_forward				5′-GGAGGAGGGGTACAGAAACG-3′
THBS1_reverse	7057	NM_003246.3		5′-CAGGCATCCATCAATTGGACAG-3′
THBS1_ probe			FAM	5′-ACCCCAGTTTGGAGGCAAGGACTGCGT-3′
FN1_forward			—	5′-GGCTGGAGCCGGGCATTGAC-3′
FN1_reverse	2335	NM_212482.1	—	5′-GGGAGGAGGAACAGCCGTTTGTT-3′
FN1_probe			Tx Red	5′-TGTAGTAGGGGCACTCTCGCCGCCA-3′
MMP12_forward				5′-TGCCCGTGGAGCTCATGGAGAC-3′
MMP12_reverse	4321	NM_002426.4		5′-CCTCCAATGCCAGATCCAGGTCCAA-3′
MMP12_ probe			HEX	5′-AGCATGGGCTAGGATTCCACCTTTGCCATCA-3′
PDGFD_forward				5′-CCTCAGGCGAGATGAGAGCAATCAC-3′
PDGFD_reverse	80310	NM_025208.4		5′-TTCCTGGGGTAGCTGTTCGGGA-3′
PDGFD_ probe			Cy5	5′-TGCACGTAGCCGTTTCCTTTCACCTGG-3′
GNB2L1_forward			—	5′-CCAGCAGCAAGGCAGAACCACC-3′
GNB2L1_reverse	10399	NM_006098.4	—	5′-ACACTCGCACCAGGTTGTCCG-3′
GNB2L1_probe			Cy5.5	5′-TGCACCTCCCTGGCCTGGTCTGCT-3′

The primers and probes specific for CHI3L1, COL6A2, MMP7, MMP9; IGF1, IGFBP2, SPP1, THBS1; and FN1, MMP12, PDGFD were collectively used in multiplex-1, -2, and -3, respectively. The primers and probe specific for GNB2L1, our reference gene,[E1] were added into each multiplex.

Cy, Cyanine; *FAM*, fluorescein; *GNB2L1*, guanine nucleotide-binding protein, β-polypeptide 2-like 1; *HEX*, hexachloro-fluorescein; *Tx Red*, Texas Red.

TABLE E2. Timing of BAL sample collection in patients with multiple lavages

	0.5-3*	3-6	6-12	12-24	Total samples
Pat. 1†		1	1		2
Pat. 2	2	1			3
Pat. 3	2	2	2		6
Pat. 4	2	1			3
Pat. 5		2			2
Pat. 6	2	2			4
Pat. 7	2	1			3
Pat. 8	2	2	2		6
Pat. 9	2				2
Pat. 10	2	1			3
Pat. 11	2	2			4
Pat. 12	2				2
Pat. 13	1	2	1		4
Pat. 14			1	1	2
Pat. 15			1	1	2
Pat. 16	1	1			2
Pat. 17	2	1	1		4
Pat. 18	2	2	1		5
Pat. 19	1	1			2
Pat. 20	1	1	1		3
Pat. 21	2				2
Pat. 22		2	2	1	5
Pat. 23	2	1	1		4
Pat. 24				2	2
Pat. 25	2	2	1		5
Pat. 26	2	2	1		5
Pat. 27	1	2	1		4
Pat. 28	2	1	1	1	5
Pat. 29				2	2
Pat. 30		1	1		2
Pat. 31		1	1		2
Pat. 32		1	1		2
Pat. 33		1	1		2
Pat. 34		1	1		2

*Time window posttransplantation (months).
†Patient code.

TABLE E3. Sample distribution based on transbronchial biopsy evaluation*

	Grade	Low	Anabolic	Intermediate	Catabolic	Firmi/Proteo/ Actino dysbiosis	No dysbiosis	Bact dysbiosis
Acute rejection	A0	28 (80)	24 (80)	57 (86.4)	13 (81.3)	20 (87)	84 (81.5)	24 (92.3)
	A1 (minimal)	5 (14.3)	6 (20)	7 (10.6)	3 (18.7)	3 (13.0)	16 (15.6)	1 (3.8)
	A2 (mild)	2 (5.8)	0 (0)	2 (3)	0 (0)	0 (0)	3 (2.9)	1 (3.8)
Airway inflammation	B0	31 (88.6)	22 (84.6)	57 (89.1)	11 (78.6)	13 (72.2)	69 (84.1)	20 (95.2)
	B1-B2 (low grade)	4 (11.4)	4 (15.4)	7 (10.9)	3 (21.4)	5 (27.8)	13 (15.9)	1 (4.8)

Data presented as n (%) within each BAL cell gene expression profile or microbiota composition group.
Actino, Actinobacteria; *Bact*, Bacteroidetes; *Firmi*, Firmicutes; *Proteo*, Proteobacteria.
*Grading of pulmonary allograft rejection according to guidelines of the International Society for Heart and Lung Transplantation.[E3]